A Calibration-Free Method for the Dielectric Constant Calculation of Low-Loss Materials

Hassan Shwaykani, *Student Member, IEEE*, Ali El-Hajj, Joseph Costantine, *Senior Member, IEEE*, and Mohammed Al-Husseini, *Member, IEEE*

***Abstract*— This article presents a new method for the calculation of the dielectric constant of low-loss materials having a thickness of more than half a wavelength in the sample. The proposed method relies solely on the frequency values at which the reflection coefficient S_{11} resonance occurs and does not require precalibration or shifting of the reference measurement plane from the input port to the material under test (MUT) air interface. The method is analyzed and tested for a large set of dielectric materials, where the accurate estimation of their electric permittivity is obtained. It is valid for scenarios where the MUT is inside a waveguide transmission line and can be extended to materials inserted in a transverse-electromagnetic (TEM) transmission line, such as in a coaxial cable. This method can be integrated into different sensors used for permittivity measurements of low-loss dielectrics and to provide the transition between the measured wave reflection coefficient and sample permittivity.**

***Index Terms*— Dielectric constant, low-loss materials, precalibration, scattering parameters, transmission line.**

I. Introduction

PERMITTIVITY measurement using radio frequency waves is a useful and nondestructive tool for the characterization of dielectric materials. Its applicability arises from the fact that each material, such as a dielectric substrate, has a frequency-specific dielectric footprint that varies with respect to its composition or state [1]–[3]. Such variation can be associated with factors, such as temperature, pressure, mixture concentration, water percentage, or others. Measurement methods that have been developed throughout the years are classified into resonant and nonresonant. Resonant methods provide accurate measurement of the dielectric properties of materials over a narrow frequency range [4]–[7], whereas nonresonant methods reveal less accurate information over a wider frequency range [7]–[12].

Manuscript received November 24, 2019; revised May 1, 2020; accepted July 10, 2020. Date of publication July 24, 2020; date of current version November 25, 2020. This work was supported in part by the National Council for Scientific Research in Lebanon (CNRS-L); and in part by the American University of Beirut (AUB). The Associate Editor coordinating the review process was Kamel Haddadi. *(Corresponding author: Joseph Costantine.)*

Hassan Shwaykani, Ali El-Hajj, and Joseph Costantine are with the Department of Electrical and Computer Engineering, American University of Beirut, 1107 2020 Beirut, Lebanon (e-mail: hms53@aub.edu.lb; elhajj@aub.edu.lb; jc14@aub.edu.lb).

Mohammed Al-Husseini is with the Beirut Research and Innovation Center, Lebanese Center for Studies and Research, 2052 6703 Beirut, Lebanon (e-mail: husseini@ieee.org).

Digital Object Identifier 10.1109/TIM.2020.3011765

One of the commonly used nonresonant methods is the transmission/reflection method. In this case, the material under test (MUT) is inserted into a section of a rectangular waveguide or a coaxial transmission line. The measured reflection and transmission coefficients (S_{11} and S_{21}) are then used to obtain the electric permittivity of the MUT through different calculation methods. Each one of these methods has its own limitations and constraints. The Nicolson–Ross–Weir (NRW) method [13], [14] is commonly used and provides an accurate estimation of the electric permittivity of low-loss materials having a thickness of less than half a wavelength in the sample, but it diverges at frequencies corresponding to integer multiples of one-half guided wavelength ($\lambda_g/2$) when the sample thickness exceeds the ($\lambda_g/2$) limit. The proposed solutions to this problem [15]–[17] rely in most cases on phase measurements, which require accurate calibration to shift the measurement reference plane to the proper position.

In this article, a new technique is presented to calculate the dielectric constant of low-loss materials having a sample thickness of more than ($\lambda_g/2$), using the measured magnitude of the reflection coefficient S_{11} solely, and without the need for any precalibration process. The proposed method is a conversion technique, rather than a characterization method. It enables the transition between the measured scattering parameters and the electrical properties of the MUT.

The novelty of the work presented in this article is its independence from calibration requirements. The proposed technique has low sensitivity to errors introduced by the measurement setup that typically cannot be avoided without precalibration measurements. This is due to the fact that our method is based on the resonances identified in the magnitude of the reflection coefficient S_{11}. Such calibration transparency provides the method with the required flexibility and allows its employment in a wider range of scenarios, especially in setups where calibration measurements are not possible or easy to execute. Section II of this article describes the theoretical background of the proposed technique. Section III presents the simulation test bench, the measurements setup, and the calculated dielectric constants that are validated against their reference values. Concluding remarks are given in Section IV.

II. Theory and Procedure

The proposed technique relies solely on the frequency values at which the reflection coefficient S_{11} resonance occurs.

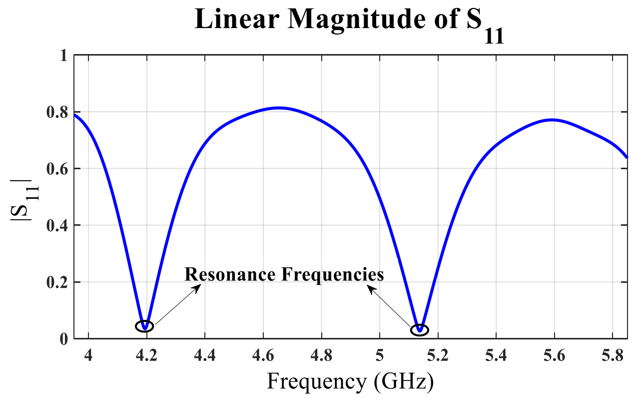

Fig. 1. Example of a linear magnitude of S_{11} for a Rogers RO3006 sample inserted in a WR187 waveguide as a function of frequency showing two resonance points.

It is, therefore, insensitive to any variation in S_{11} and S_{21} phases caused by different adapters and cables used in the measurement setup. This eliminates the need for any calibration process prior to measurements, which is helpful in scenarios where calibration [thru, reflect, and line (TRL) or other] is hard to perform, such as in free space measurements, or transverse-electromagnetic (TEM) cells.

In the case of MUTs with thicknesses beyond $(\lambda_g/2)$, the reflection coefficient exhibits a resonance ($S_{11} = 0$) at frequencies that correspond to integer multiples of $(\lambda_g/2)$ [16]. Fig. 1 shows an example of the resonance points in the simulated reflection coefficient S_{11} of a Rogers RO3006 sample with a thickness of 60 mm placed inside a WR187 waveguide. This condition is valid for low-loss materials, but cannot be guaranteed for high-loss ones. Hence, our method is restricted to low-loss materials only, and it will use these resonance points to calculate an intermediate variable denoted by m, which is then used to calculate ε_r over the entire operating frequency range.

A. Intermediate Variable m

For a given permittivity measurement, the thickness d of the sample under test is constant (d = constant), and the term $(2d/\lambda_g)$ is, therefore, a function of the frequency f. We define the variable $m(f)$ to be

$$m(f) = \frac{2d}{\lambda_g}. \tag{1}$$

The first two consecutive resonance frequencies are denoted as f_{r1} and f_{r2}. Given that each resonance corresponds to the frequency where the material thickness is integer multiple of $(\lambda_g/2)$, and if f_{r1} corresponds to $k \times (\lambda_g/2)$, then f_{r2} corresponds to $(k+1)\times(\lambda_g/2)$. Therefore, the integer variables $m(f_{r1})$ and $m(f_{r2})$ satisfies the following condition:

$$m(f_{r2}) - m(f_{r1}) = 1. \tag{2}$$

Assuming that the MUT is a low-dispersive material, we can, therefore, derive a linear approximation for $m(f)$ in terms of f_{r1}, f_{r2}, and $m(f_{r1})$

$$m(f) = \frac{f - f_{r1}}{f_{r2} - f_{r1}} + m(f_{r1}). \tag{3}$$

Given that λ_g and $m(f_{r1})$ are unknown, (3) shows that if we calculate $m(f_{r1})$, then we can conclude $m(f)$, which can be used later on to determine the value of $\varepsilon_r(f)$ over the entire working frequency band.

B. Iterative Calculation of m(fr1)

In this part, the steps to be applied in each iteration are shown, with the index i referring to the ith iteration. The iterative procedure starts at $i = 1$ and ends, as instructed in the following.

Step 1: Suppose that $m(f_{r1}) = i$.

Step 2: Calculate $m(f)$ using (3) with the assumption stated in the previous step.

Step 3: Use the relations between λ_g and ε_r for a nonmagnetic material ($\mu_r = 1$) inserted in a rectangular waveguide transmission line operating in TE_{10} mode (with width $= a$) that is given by [18], where λ_0 is the free space wavelength

$$\lambda_g = \frac{2\pi}{\sqrt{\frac{4\pi^2 f^2 \varepsilon_r}{c^2} - \left(\frac{\pi}{a}\right)^2}} \tag{4}$$

$$\varepsilon_r(f) = \left(\frac{\lambda_o}{\lambda_g}\right)^2 + \left(\frac{\lambda_o}{2a}\right)^2. \tag{5}$$

Equations (1) and (5) can be rearranged and then combined into an approximate expression of ε_r in terms of $n(f)$, f, d, a, and c (speed of light) as given by [18]

$$\varepsilon_r(f) = \left(\frac{m(f)\times c}{2d \times f}\right)^2 + \left(\frac{c}{2a \times f}\right)^2. \tag{6}$$

Calculate the value of $\varepsilon_r(f)$ at all frequencies using (6).

Step 4: Equation (4) can be rearranged to obtain the following expression of f:

$$f = \frac{c}{\sqrt{\varepsilon_r(f)}} \times \sqrt{\frac{1}{\lambda_g(f)^2} + \frac{1}{4a^2}}. \tag{7}$$

Step 5: Now we will assume that the calculated value of $\varepsilon_r(f)$ is the true value, and we will use it to calculate the value of resonance frequencies $f_{r1,\mathrm{cal}}$ and $f_{r2,\mathrm{cal}}$

$$f_{r1\mathrm{cal}} = \frac{c}{\sqrt{\varepsilon_r(f_{r1\mathrm{cal}})}} \times \sqrt{\frac{1}{\lambda_g\left(f_{r1,\mathrm{cal}}\right)^2} + \frac{1}{4a^2}} \tag{8}$$

where $\lambda_g(f_{r1,\mathrm{cal}})$ is equal to $(2d)/(m(fr1))$ and $\varepsilon_r(f_{r1,\mathrm{cal}})$ is approximated by $\varepsilon_{r,\mathrm{avg}} = \mathrm{mean}(\varepsilon_r(f))$. The value of $f_{r2,\mathrm{cal}}$ is calculated in the same way.

Step 6: Compare the calculated values $f_{r1,\mathrm{cal}}$ and $f_{r2,\mathrm{cal}}$ to the actual values f_{r1} and f_{r2}. If they are equal, then the initial assumption made in step 1 is true. If not, move to the next iteration and repeat the same steps.

For this purpose, the relative error between the actual and calculated resonance frequencies are denoted as $e_{1,i}$ and $e_{2,i}$

$$e_{1,i} = \frac{\Delta f_{r1}}{f_{r1}} = \frac{|f_{r1} - f_{r1,\text{cal}}|}{f_{r1}} \tag{9}$$

$$e_{2,i} = \frac{\Delta f_{r2}}{f_{r2}} = \frac{|f_{r2} - f_{r2,\text{cal}}|}{f_{r2}}. \tag{10}$$

If $e_{1,i}$ and $e_{2,i}$ are approximately equal to zero, then the assumption made in step 1 is true, and the value of $m(f_{r1})$ is successfully calculated. If not, move to the next iteration.

Step 7: Repeat steps 1–6 until $f_{r1,\text{cal}}$ and $f_{r2,\text{cal}}$ converge to the actual f_{r1} and f_{r2} values.

C. Dielectric Constant ε_r

Finally, substitute the expression of $m(f)$ given by (3) in (6), and then use the value of $m(f_{r1})$ calculated in Section II-B to determine the value of the dielectric constant of the MUT at all frequencies using the following:

$$\varepsilon_r(f) = \left(\frac{\left(\frac{f-f_{r1}}{f_{r2}-f_{r1}} + m(f_{r1})\right) \times c}{2d \times f}\right)^2 + \left(\frac{c}{2a \times f}\right)^2. \tag{11}$$

Equation (11) shows that the proposed method provides the value of ε_r only, without the loss tangent ($\tan\delta$) value. This is due to the fact that this method solely relies on the magnitude of S_{11} as an input. Thus, a tradeoff occurs that forces the user to sacrifice the calculation of $\tan\delta$, while benefiting from immunity to phase changes. Hence, phase variations are transparent to this technique. In addition, a major benefit results from calculating the dielectric constant of any low-loss MUT using noncalibrated S_{11} measurements. Although a small error is introduced to the value of $|S_{11}|$ if no calibration is done, this error has no significant effect on the calculated value of $\varepsilon_r(f)$ as is also demonstrated experimentally.

III. Experimental Results

In this section, the proposed calculation method is tested over the rectangular waveguide characterization method. For this purpose, the sample under test is inserted in a WR187 waveguide, and the reflection coefficient S_{11} is measured then fed in the method to calculate the dielectric constant of the MUT. The accuracy of the proposed method is evaluated using a set of sample MUTs with known dielectric constants that are used in a CST microwave studio [19] simulation test bench in addition to real measurement setups. Both simulation and measurements are done for two cases: with and without calibration. "With calibration" refers to the case where the reference measurements plane is shifted from the input port to the MUT-air interface. The reason for having these two cases is to differentiate between the calculation error induced by the method and the additional error due to the lack of calibration.

A. Simulation Test Bench

Multiple scenarios for multiple MUTs with known dielectric constants are simulated when each MUT is inserted in a WR187 waveguide section. The various samples used are listed in Table I, along with their approximate dielectric constants and thickness values. The magnitude of the reflection coefficient S_{11} is then obtained. Magnitude values are then used to identify the resonant frequencies, which are substituted in (11) in order to obtain the dielectric constant value. The calculated MUT's permittivity is then compared with its reference value obtained from the simulator's material library, where the used electric dispersion model is CST's Nth order model (the Debye–Lorentz dispersion model) [20].

TABLE I
SAMPLES CHARACTERISTICS

Sample	Dielectric Constant	Thickness (mm)
PMMA (Acrylic glass)	~2.6	60
PLA Plastic (Polylactic Acid)	2.55-2.65	60
Ice	3.12	60
FR4	4.3	60
Rogers RO3006	6.15	60

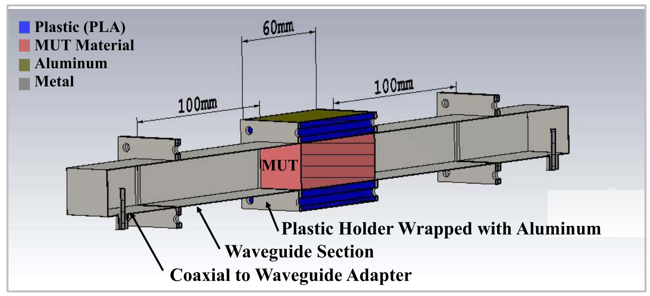

Fig. 2. EM simulation (CST) test bench cross section view showing different components.

Fig. 2 shows the test bench that was used and simulated to compute the magnitude of the reflection coefficient of the 60-mm-thick MUTs in C-band (3.95–5.85 GHz). The setup includes two coaxial to waveguide adapters that are used to excite the TE_{10} mode of the WR187 waveguide sections (47.55 mm $\times$ 22.15 mm). It also includes a sample holder that is a waveguide section that incorporates within its internal walls, the MUT, as shown in Fig. 2. The sample holder is also placed between the two waveguide sections in a tight configuration. Fig. 3 shows the simulated S_{11} magnitude of a 60-mm PLA sample inserted in a WR187 waveguide section for both cases with and without calibration. Different resonance frequencies shown in Fig. 3 are then used to calculate the dielectric constant of the sample. Fig. 4 shows the calculated permittivity ($\varepsilon_{\text{calculated}}$) along with the percentage error (%E_{rror}) of the dielectric constant estimation for the PLA sample. $\varepsilon_{\text{calculated}}$ and %E_{rror} for PMMA sample are shown in Fig. 5, while those for Ice, FR4, and Rogers RO3006 are shown in Figs. 6–8, respectively. Such results are obtained without calibration and compared with the results obtained when calibration is performed. Calibration, in this case, is done using TRL calibration standards. One MUT measurement and three calibration measurements that make up the TRL

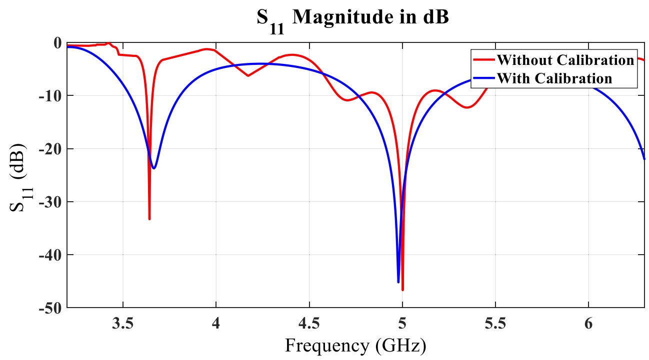

Fig. 3. Simulated S_{11} magnitude of PLA sample inserted in a WR187 waveguide section for both cases with and without calibration, showing the different resonance frequencies.

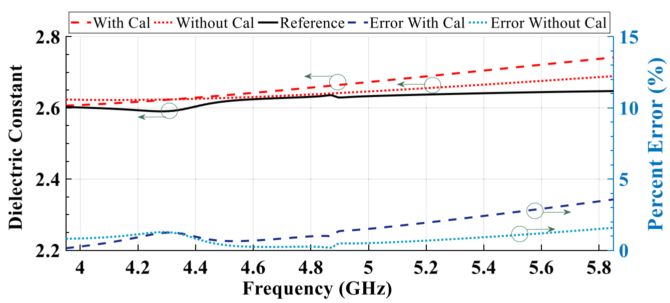

Fig. 4. Calculated dielectric constant (left axis) of PLA sample with and without calibration versus reference value, along with the percent error in calculated dielectric constant (right axis).

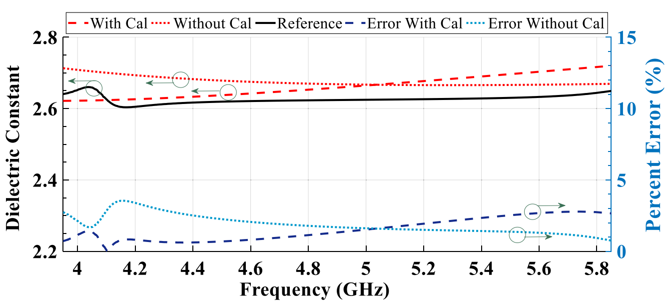

Fig. 5. Calculated dielectric constant (left axis) of PMMA sample with and without calibration versus reference value, along with the percent error in calculated dielectric constant (right axis).

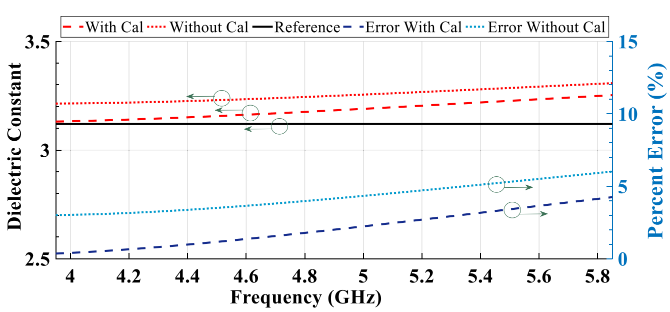

Fig. 6. Calculated dielectric constant (left axis) of Ice sample with and without calibration versus reference value, along with the percent error in calculated dielectric constant (right axis).

calibration standards are performed. For the "thru" measurement, the transmitting and receiving waveguide ends are connected to each other, as shown in Fig. 9(a). For the "line"

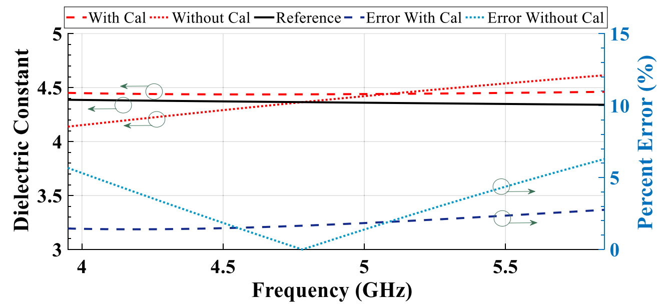

Fig. 7. Calculated dielectric constant (left axis) of FR4 sample with and without calibration versus reference value, along with the percent error in calculated dielectric constant (right axis).

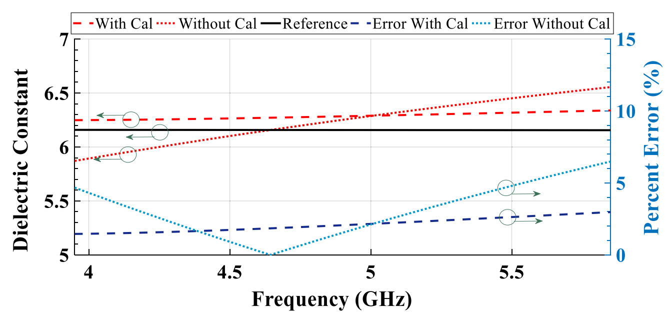

Fig. 8. Calculated dielectric constant (left axis) of Rogers RO3006 sample with and without calibration versus reference value, along with the percent error in calculated dielectric constant (right axis).

measurement, a $\lambda/4$ line (known as a spacer) is placed between the waveguide ends, as shown in Fig. 9(b). For the "reflect" measurement, the transmitting and receiving waveguides are connected one at a time to a short plate placed $\lambda/4$ apart from the waveguide, as shown in Fig. 9(c). These calibration measurements allow moving the calibration reference plane from the coaxial port to the waveguide ends. Therefore, after simulating the scattering parameters for these three different scenarios, as shown in Fig. 10, we simulate the scattering parameters for the MUT using the setup shown in Fig. 2. Then, we use the results as an input to a postprocessing TRL calibration code in order to calculate the values of the de-embedded S-parameters that represent the calibrated S-parameters. The TRL calibration code is based on the details discussed in [21].

It is concluded that for these five different materials (PLA, PMMA, Ice, FR4, and Rogers RO3006), the permittivity of the low-loss MUTs having a large thickness is calculated with a 96% accuracy when a proper calibration process (TRL calibration) is done. The permittivity is calculated with 93% accuracy if no calibration is done. In addition, no divergence occurs at frequencies corresponding to integer multiples of half-wavelength in the sample. The results show a stable response over the waveguide's operation range.

The error in the case where calibration is applied can be linked to the use of different mathematical assumptions and approximations in the theoretical development of the method, in particular in (3) and (8)–(10) when $e_{1,i}$ and $e_{2,i}$

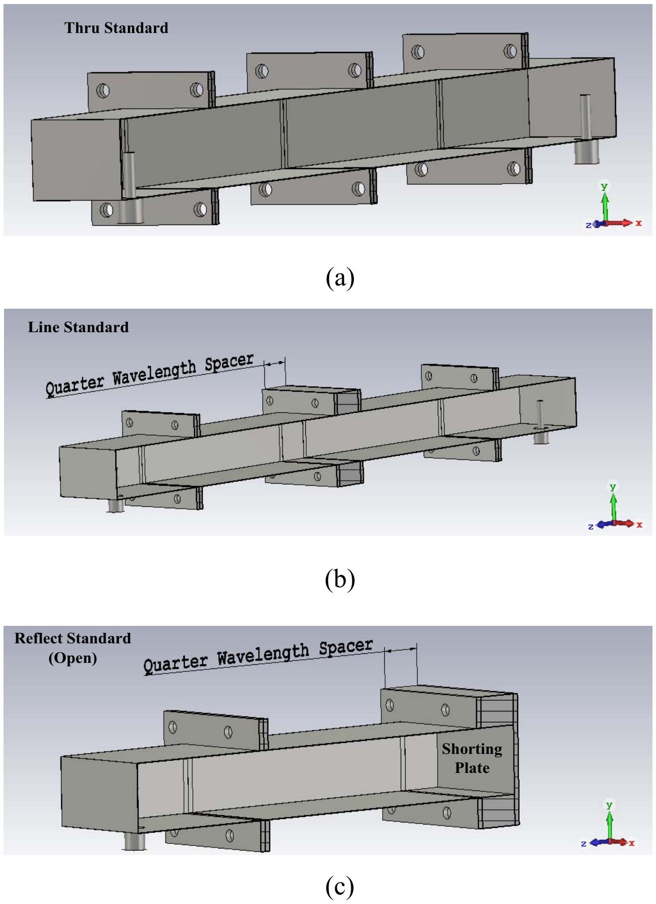

Fig. 9. Cross-sectional view of different setups used to perform TRL Calibration. (a) Thru standard. (b) Line standard. (c) Reflect (open) standard.

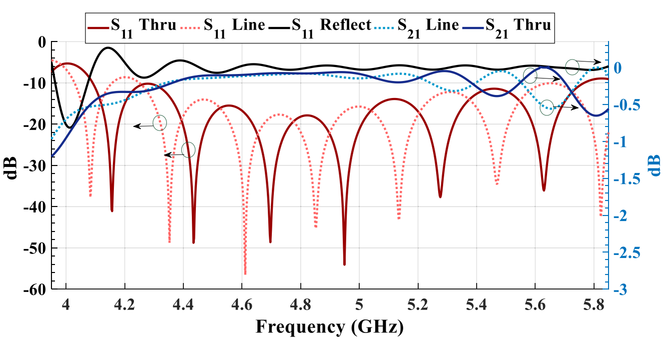

Fig. 10. Simulated S-parameters magnitude of the Thru, Line, and Reflect calibration standards.

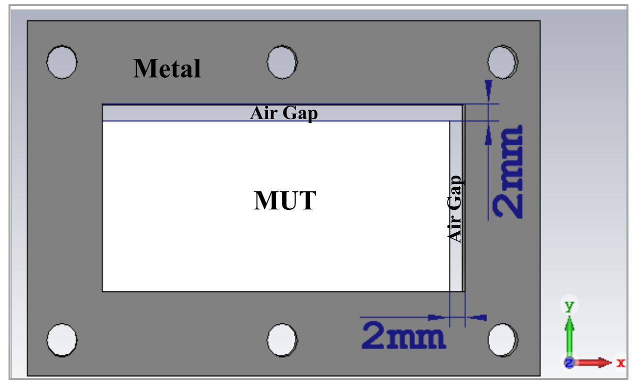

Fig. 11. Cross section view of the air gap between MUT and waveguide sample holder.

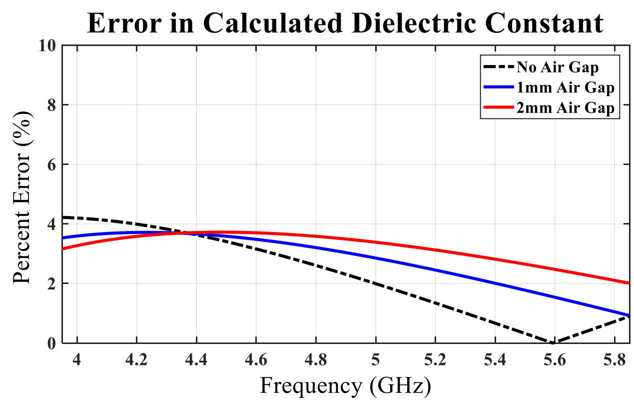

Fig. 12. Percent error in calculated dielectric constant of Teflon sample, without calibration for different air gap values.

are approximated to zero. On the other hand, the error in the case where no calibration is applied can be linked—in addition to the method's approximations and assumptions—to the uncertainties added due to the lack of calibration, i.e., uncertainties caused by the imperfect values of the non-calibrated S_{11} resonance, which are measured without a proper shift of the reference plane. The effect of air gaps between the sample MUT and the walls of the waveguide sample holder on the accuracy of the method is considered. This study is performed in order to investigate the effect of the errors in MUT machining (i.e., the process of cutting the MUT with the dimensions of a WR187 waveguide section in order to fit it inside the sample holder) on the accuracy of the calculated dielectric constant. For this purpose, air gaps up to 2 mm are simulated, as shown in Fig. 11, and the accuracy obtained is in the same range as in the absence of air gaps. Fig. 12 shows the $\%\mathrm{E}_{\mathrm{rror}}$ in the calculated dielectric constant of Teflon sample (without calibration) for different air gap values. The graph shows that even with a 2-mm air gap, a 93%–96% accurate results can still be guaranteed. In other words, errors up to 2 mm in MUT machining have no effect on the accuracy of the calculated dielectric constant.

In order to evaluate the performance of the method with respect to higher loss materials, simulations for an MUT with a constant dielectric constant ($\varepsilon_r = 2.1$), and a variable loss tangent are performed. It is assumed that the loss tangent is varying between 0 and 0.2, with a step of 0.01. This evaluation is executed in order to estimate the accuracy of the proposed method in determining the dielectric properties for materials with a high-loss tangent. Fig. 13 shows the linear magnitude of S_{11} for different values of the loss tangent ($c =$ loss tangent value) for a 60-mm sample with a variable loss tangent. We can notice that for higher loss tangent values, S_{11} resonance frequencies do not vary. However, after a certain limit, the S_{11} magnitude increases, which results in the resonance frequencies becoming unidentifiable. Thus, these

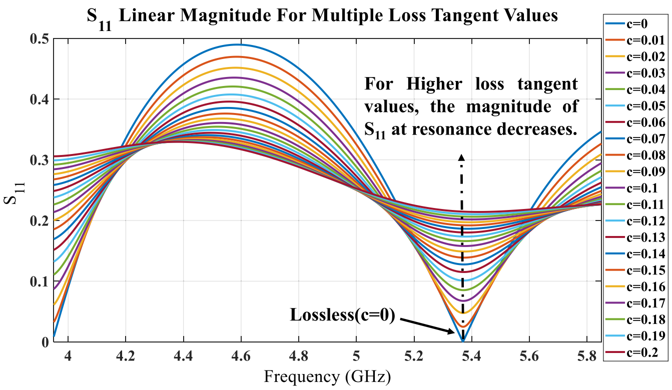

Fig. 13. S_{11} linear magnitude versus frequency for different values of loss tangent for a 60-mm-thick sample with $\varepsilon_r = 2.1$.

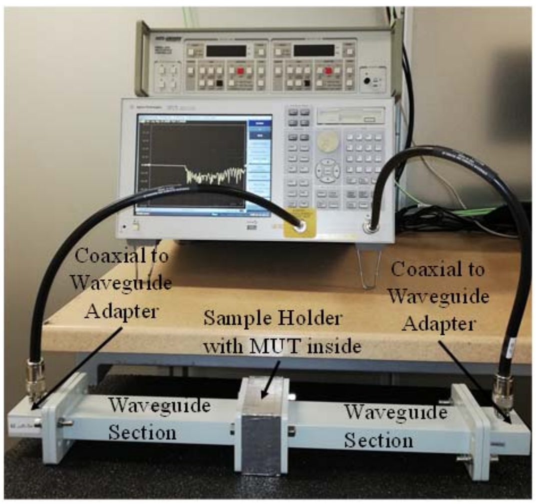

Fig. 14. Measurements setup for MUT characterization.

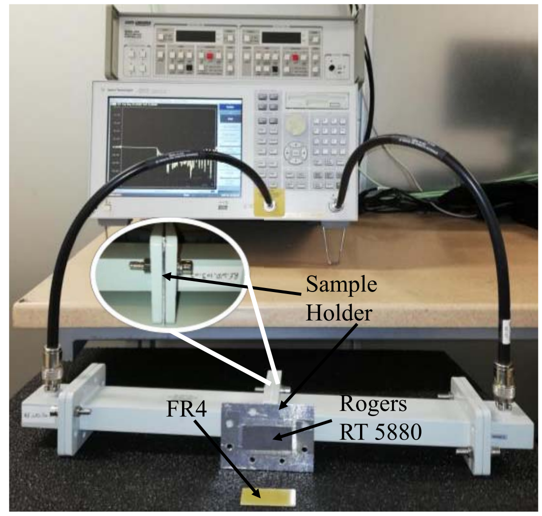

Fig. 15. Setup for reference value measurements.

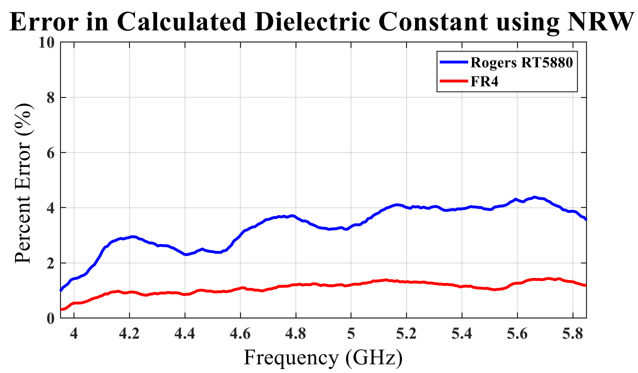

Fig. 16. Percent error in calculated dielectric constant of Rogers RT5880 and FR4 samples using the NRW method.

undetermined resonances can no longer be used in the proposed method. Thereby, this method is limited to loss tangents that are less than 0.1, where resonances can remain clear, and the same accuracy is maintained.

B. Measurements Setup

In this section, the setup shown in Fig. 14 is used to perform measurements on different sample MUTs to calculate their dielectric constant in C-band (3.95–5.85 GHz), and thus, evaluate the accuracy of the method. The measurement setup mirrors the one represented in the simulation environment. The measurement setup includes two coaxial to WR187 waveguide adapters that are connected to two 20-cm WR187 waveguide sections, as shown in Fig. 14. Between the two waveguide sections, the MUT is fitted inside a sample holder. In this setup, the sample holder is a 3-D printed plastic sample holder having the inner dimensions of a WR187 rectangular waveguide (47.55 mm $\times$ 22.15 mm) with a thickness equal to that of the sample MUT (40 and 60 mm). The 3-D printer used is CREALITY CR-10 [22]. The plastic holder is wrapped from inside and outside with conductive adhesive aluminum tape, where continuous contact in ensured and verified experimentally. The aluminum wrapping is smoothed and has a thickness of 0.2 mm, above the required skin depth. As a result, the 3-D holder now acts as aluminum-made waveguide section with the same inner and outer dimensions of a typical commercially available WR187 MUT holder. The holder with the MUT inside is placed between the two WR187 waveguide sections. $|S_{11}|$ is then measured using a vector network analyzer (VNA) and fed into the method to calculate the dielectric constant of each sample. The calculated dielectric constant value is then compared with the reference value to determine the method's accuracy. The NRW method is used to determine the reference value of each sample in order to correlate it with the information provided by the manufacturer. The reliability of the NRW code in estimating accurate dielectric values of the material is first tested, as shown in Fig. 15, for two MUT samples with known dielectric constants and thickness. These dielectric materials are FR4 and Rogers RT5880, respectively, having each a thickness of 1.6 mm. Such a thickness is chosen in order to ensure that NRW results do not diverge. For these two cases, the values of S_{11} and S_{21} are measured after running TRL calibration and, then, are used as inputs to the NRW code. The results are compared with the reference values given by the manufacturer. Fig. 16 shows that the used NRW code provides an accurate estimation of the permittivity value and can be relied upon as a reference.

TABLE II
SAMPLES' CHARACTERISTICS

Sample	Dielectric Constant	Thickness (mm)
PMMA (Acrylic glass)	~2.6	60
PLA Plastic (Polylactic Acid)	2.55-2.65	60
Ice	3.12	40

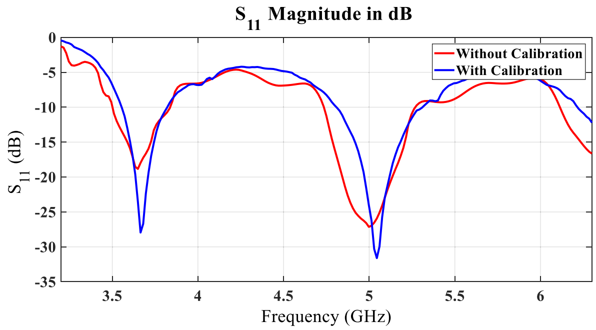

Fig. 17. Measured S_{11} magnitude of PLA sample inserted in a WR187 waveguide section for both cases with and without calibration, showing the different resonance frequencies.

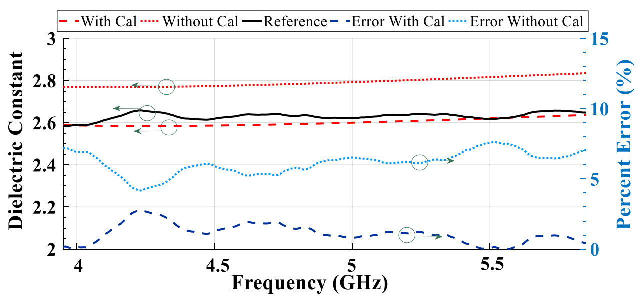

Fig. 18. Calculated dielectric constant (left axis) of PLA sample with and without calibration versus reference value, along with the percent error in calculated dielectric constant (right axis).

Three measurements are then done for each of the three available MUT samples shown in Table II. The first one is the reference measurement, and it is done on a thin version of the sample MUT (~5 mm), where S_{11} and S_{21} are measured then used along with NRW to calculate the reference permittivity value of the material as recorded in Table II. The other two measurements are used to evaluate the accuracy of the method: one measurement is completed with TRL calibration, in order to shift the measurement's reference plane from the port of the VNA to MUT-air interface. The second measurement is executed without calibration. In the last two measurement scenarios, only the magnitude of S_{11} is noted, and then it is used to identify the resonant frequencies. These resonant frequencies are then integrated into (11), in order to extract the corresponding value of the dielectric constant of each MUT.

Fig. 17 shows the measured S_{11} magnitude of a 60-mm PLA sample inserted in a WR187 waveguide section for both cases with and without calibration. The calculated permittivity ($\varepsilon_{\text{calculated}}$), along with the %$\text{E}_{\text{rror}}$ of the dielectric constant estimation for the PLA sample, is shown in Fig. 18.

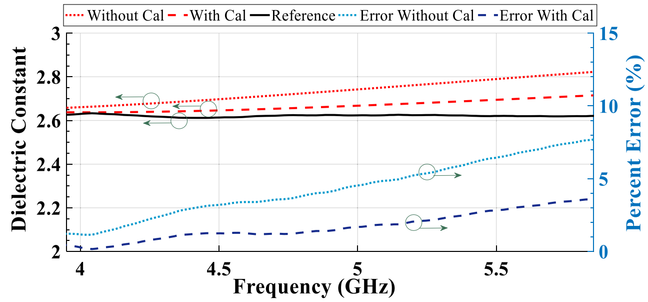

Fig. 19. Calculated dielectric constant (left axis) of PMMA sample with and without calibration versus reference value, along with the percent error in calculated dielectric constant (right axis).

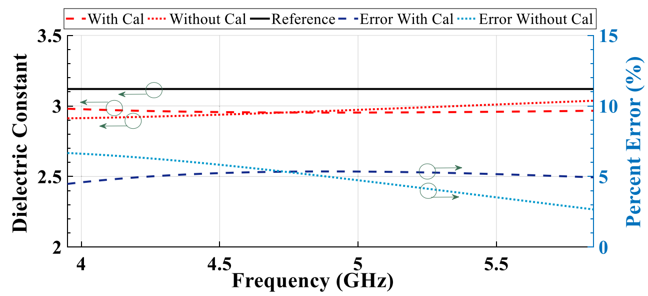

Fig. 20. Calculated dielectric constant (left axis) of Ice sample with and without calibration versus reference value, along with the percent error in calculated dielectric constant (right axis).

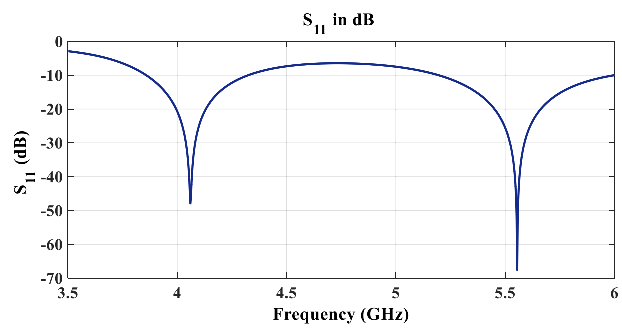

Fig. 21. Simulated S_{11} magnitude of a 60-mm Teflon sample with $\varepsilon_r = 2.1$ inserted in a WR187 waveguide section for the case with calibration, showing the different resonance frequencies.

$\varepsilon_{\text{calculated}}$ and %E_{rror} for PMMA and Ice samples are shown in Figs. 19 and 20, respectively.

Such results are obtained without calibration and compared with the results obtained when calibration is performed.

These results prove that the method can be used to calculate the dielectric constant of low-loss MUTs having a thickness of more than $(\lambda_g/2)$ with 95% accuracy if a proper calibration process is done. Furthermore, it proves that the proposed method can calculate the dielectric constant of a low-loss MUT with 92% accuracy in the absence of any calibration. In addition, these measurements validate the simulation results by verifying that no divergence occurs at frequencies corresponding to integer multiples of half-wavelength in the sample. In addition, it is important to note that the calculated results are stable over the waveguide's operating range. Table III presents

TABLE III
COMPARISON BETWEEN THE PROPOSED METHOD AND THE COMMON CONVERSION METHODS

	NRW [13-14]	NIST ITERATIVE [15]	NEW NON-ITERATIVE [16]	Proposed Method
Need for Initial Guess	No	Yes	No	No
Iterative	No	Yes	No	Semi
Constraints on MUT thickness	Short sample should be used	Arbitrary length of samples can be used	Arbitrary length of samples can be used	Long sample should be used
Measured parameters	Permittivity, Permeability	Permittivity	Permittivity	Dielectric Constant
MUT type	High Loss, Low-Loss (Short Sample)	High Loss, Low Loss	High Loss, Low Loss	Low-Loss
Smooth vs Divergence (sharp variation from true value)	Divergence at frequencies corresponding to multiples of one-half wavelength	Smooth, No Divergence	Smooth, No Divergence	Smooth, No Divergence
Need for Calibrated S-parameters	Yes	Yes	Yes	No

TABLE IV
COMPARISON BETWEEN THE PROPOSED METHOD AND THE METHOD IN [18]

	THIS PAPER	Method Proposed in [18]
Convergence	**Converges** even in the presence of a shift in measured resonance frequencies.	**Diverges** in the presence of a small shift in measured resonance frequencies
Sensitivity	**Same sensitivity** in case no shift in measured resonance frequency since they have same error range. However, **higher sensitivity** in case a frequency shift occurs.	**Same sensitivity** in case no shift in measured resonance frequency since they have same error range. However, **lower sensitivity** in case a frequency shift occurs.
Repeatability	**Outperforms [18]**, since for multiple measurements, the resonance frequencies may shift, and the method is immune to small frequency shifts	In case of a small frequency shift between successive measurements, [18] may diverge.
Measurement time	Preparation, Measurement, and Post processing times are almost the **same** as [18]	Preparation, Measurement, and Post processing times are almost the **same** as the proposed method
Accuracy	**Same accuracy** under perfect conditions with no shift in measured resonance frequency. However, **higher accuracy** in case a frequency shift occurs.	**Same accuracy** under perfect conditions with no shift in measured resonance frequency. However, **lower accuracy** in case a frequency shift occurs.

a comparison between this work's proposed method and popular methods available in the literature based on selected key factors. Factors, such as MUT constraints, size, measured parameters, and most importantly, the flexibility of the method and its ability to overcome the need for calibrated S-parameters measurements, are summarized. The method proposed herein is compared with the method discussed in [18] for the same MUT and within the same setup. It is proven that the method proposed in this article is more robust and more reliable than the one in [18] when it comes to small shifts in the measured resonant frequencies. From Fig. 21, the resonance frequencies are determined to be $f_{r1} = 4.06$ GHz and $f_{r2} = 5.55$ GHz. Applying these resonance frequencies on the method proposed in [18] and the method proposed in this article will result in

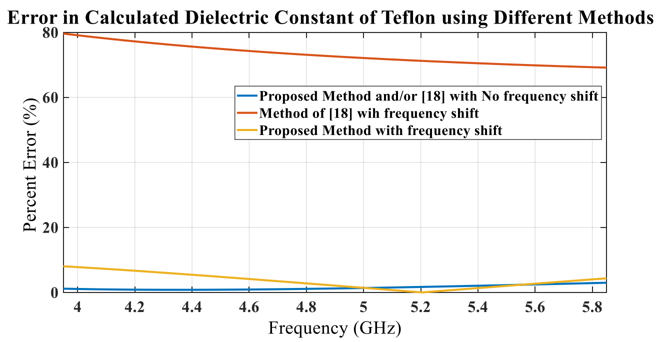

Fig. 22. Percent error in the calculation of the dielectric constant of Teflon sample using method of [18] in cases of no shift in the measured resonance frequencies ($f_{r1} = 4.06$ GHz and $f_{r2} = 5.55$ GHz) and in case of a small shift in the measured resonance frequencies ($f_{r1} = 4.22$ GHz and $f_{r2} = 5.55$ GHz).

the accurate estimation of the dielectric constant of the MUT, which is clearly demonstrated in Fig. 22. If any small shift occurs in the resonance frequency estimation, for example, if f_{r1} is measured with a 4% error, the accuracy of the method proposed herein is sustained at a high level, as shown in Fig. 22. Table IV summarizes the comparison between the proposed method and the method presented in [18], in the function of convergence, sensitivity, repeatability, measurement, and accuracy. Moreover, this technique is not limited to the waveguide characterization method, but it can be extended to any TEM transmission lines, such as coaxial cables.

IV. Conclusion

In this article, a new calibration-free method for the dielectric constant calculation of low-loss materials having a thickness of more than half-wavelength is proposed. The presented technique provides the transition between the measured scattering parameters and the electrical properties of the MUT. It is validated for a wide set of reference MUTs that are inserted within a WR187 rectangular waveguide. The calculated dielectric constant values are proven to be 92%–93% accurate and are stable (i.e., no divergence at frequencies corresponding to an integer multiple of half-guided wavelength) over the used waveguide's operating frequency range, with no premeasurements calibration. The proposed method can be extended to any TEM transmission line.

References

[1] *Basics of Measuring the Dielectric Properties of Materials*, Keysight Technol., Santa Rosa, CA, USA, Jan. 2019. [Online]. Available: https://www.keysight.com/zz/en/assets/7018-01284/application-notes/5989-2589.pdf

[2] G. Vlachogiannakis *et al.*, "Miniaturized broadband microwave permittivity sensing for biomedical applications," *IEEE J. Electromagn., RF Microw. Med. Biol.*, vol. 3, no. 1, pp. 48–55, Mar. 2019.

[3] S. O. Nelson and P. G. Bartley, "Measuring frequency- and temperature-dependent permittivities of food materials," *IEEE Trans. Instrum. Meas.*, vol. 51, no. 4, pp. 589–592, Aug. 2002.

[4] P. A. Bernard and J. M. Gautray, "Measurement of dielectric constant using a microstrip ring resonator," *IEEE Trans. Microw. Theory Techn.*, vol. 39, no. 3, pp. 592–595, Mar. 1991.

[5] G. Galindo-Romera, F. Javier Herraiz-Martinez, M. Gil, J. J. Martinez-Martinez, and D. Segovia-Vargas, "Submersible printed split-ring resonator-based sensor for thin-film detection and permittivity characterization," *IEEE Sensors J.*, vol. 16, no. 10, pp. 3587–3596, May 2016.

[6] H. B. Wang and Y. J. Cheng, "Broadband printed-circuit-board characterization using multimode substrate-integrated-waveguide resonator," *IEEE Trans. Microw. Theory Techn.*, vol. 65, no. 6, pp. 2145–2152, Jun. 2017.

[7] H. Shwaykani, A. El-Hajj, J. Costantine, F. A. Asadallah, and M. Al-Husseini, "Dielectric spectroscopy for planar materials using guided and unguided electromagnetic waves," in *Proc. IEEE Middle East North Afr. Commun. Conf. (MENACOMM)*, Apr. 2018, pp. 1–5.

[8] D. K. Ghodgaonkar, V. V. Varadan, and V. K. Varadan, "Free-space measurement of complex permittivity and complex permeability of magnetic materials at microwave frequencies," *IEEE Trans. Instrum. Meas.*, vol. 39, no. 2, pp. 387–394, Apr. 1990.

[9] S. Kim, D. Novotny, J. A. Gordon, and J. R. Guerrieri, "A free-space measurement method for the low-loss dielectric characterization without prior need for sample thickness data," *IEEE Trans. Antennas Propag.*, vol. 64, no. 9, pp. 3869–3879, Sep. 2016.

[10] D. V. Blackham and R. D. Pollard, "An improved technique for permittivity measurements using a coaxial probe," *IEEE Trans. Instrum. Meas.*, vol. 46, no. 5, pp. 1093–1099, Oct. 1997.

[11] A. Mirbeik-Sabzevari and N. Tavassolian, "Characterization and validation of the slim-form open-ended coaxial probe for the dielectric characterization of biological tissues at millimeter-wave frequencies," *IEEE Microw. Wireless Compon. Lett.*, vol. 28, no. 1, pp. 85–87, Jan. 2018.

[12] E. Hajisaeid, A. F. Dericioglu, and A. Akyurtlu, "All 3-D printed free-space setup for microwave dielectric characterization of materials," *IEEE Trans. Instrum. Meas.*, vol. 67, no. 8, pp. 1877–1886, Aug. 2018.

[13] A. M. Nicolson and G. F. Ross, "Measurement of the intrinsic properties of materials by time-domain techniques," *IEEE Trans. Instrum. Meas.*, vol. IM-19, no. 4, pp. 377–382, Nov. 1970.

[14] W. B. Weir, "Automatic measurement of complex dielectric constant and permeability at microwave frequencies," *Proc. IEEE*, vol. 62, no. 1, pp. 33–36, Jan. 1974.

[15] J. Baker-Jarvis, E. J. Vanzura, and W. A. Kissick, "Improved technique for determining complex permittivity with the transmission/reflection method," *IEEE Trans. Microw. Theory Techn.*, vol. 38, no. 8, pp. 1096–1103, Aug. 1990.

[16] A.-H. Boughriet, C. Legrand, and A. Chapoton, "Noniterative stable transmission/reflection method for low-loss material complex permittivity determination," *IEEE Trans. Microw. Theory Techn.*, vol. 45, no. 1, pp. 52–57, Jan. 1997.

[17] O. Luukkonen, S. I. Maslovski, and S. A. Tretyakov, "A stepwise Nicolson–Ross–weir-based material parameter extraction method," *IEEE Antennas Wireless Propag. Lett.*, vol. 10, pp. 1295–1298, 2011.

[18] H. Shwaykani, A. El-Hajj, J. Costantine, and M. Al-Husseini, "A new calculation method for the dielectric constant of low-loss materials," in *Proc. 13th Eur. Conf. Antennas Propag. (EuCAP)*, Krakow, Poland, Mar. 2019, pp. 1–3.

[19] Cst.com. (2018). *CST—Computer Simulation Technology*. [Online]. Available: https://www.cst.com/

[20] *Dassault Systèmes-CST—Computer Simulation Technology Help Contents: CST STUDIO SUITE 2019 | 2D/3D Simulation | Creating and Visualizing Models | Material Overview (HF)*, Dassault Syst., Paris, France, 2019.

[21] G. F. Engen and C. A. Hoer, "Thru-reflect-line: An improved technique for calibrating the dual six-port automatic network analyzer," *IEEE Trans. Microw. Theory Techn.*, vol. MTT-27, no. 12, pp. 987–993, Dec. 1979.

[22] Creality 3D Printers. *Creality Official: Large 3D Printer Manufacturer*. [Online]. Available: https://creality.com/

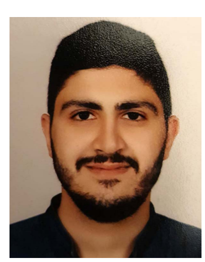

Hassan Shwaykani (Student Member, IEEE) received the B.E. degree in computer and communication engineering and the M.S. degree in microwave engineering from the Lebanese University, Beirut, Lebanon, in 2016. He is currently pursuing the Ph.D. degree in electrical and computer engineering with the American University of Beirut, Beirut, with a focus on material characterization using electromagnetic waves.

Ali El-Hajj received the M.Eng. degree from the L'Ecole Superieure d'Electricite, Gif-sur-Yvette, France, in 1981, and the Ph.D. degree in engineering from the University of Rennes 1, Rennes, France, in 1983.

He was with the Department of Electrical Engineering, Lebanese University, Beirut, Lebanon, from 1983 to 1987. He joined the American University of Beirut (AUB), Beirut, in 1987, where he is currently a Professor of electrical and computer engineering. He has 35 years of academic experience. He assumed leadership positions at AUB in General Education, Academic Program Review, Assessment of Program Learning Outcomes, Assessment of Units Outcomes, and Strategic Planning. His research interests include applied electromagnetism and machine learning.

Joseph Costantine (Senior Member, IEEE) received the bachelor's degree from the Faculty of Engineering, Branch 2, Lebanese University, Beirut, Lebanon, in 2004, the M.E. degree from the American University of Beirut, Beirut, in 2006, and the Ph.D. degree from The University of New Mexico, Albuquerque, NM, USA, in 2009.

He is currently an Associate Professor with the Department of Electrical and Computer Engineering, American University of Beirut. He holds seven provisional and full U.S. patents. He has authored or coauthored 2 books, 1 book chapter, and more than 150 journal and conference articles. His research interests reside in reconfigurable antennas, cognitive radio, RF energy harvesting systems, antennas and rectennas for IoT devices, RF systems for biomedical devices, wireless characterization of dielectric material, and deployable antennas for small satellites.

Dr. Costantine received many awards and honors throughout his career, including the 2008 IEEE Albuquerque Chapter Outstanding Graduate Award, the three year (2011–2013) Air Force Summer Faculty fellowship from the Kirtland's Space Vehicles Directorate, NM, the 2017 First Prize at the Idea-Thon of International Healthcare Industry Forum, the 2019 Excellence in Teaching Award from the American University of Beirut, and the 2018 and 2020 STC Science and Technology Innovation Awards. He has been an Associate Editor of the IEEE ANTENNAS AND WIRELESS PROPAGATION LETTERS since 2018. He was selected by the World Economic Forum as one of the World's Leading Young Scientists for the year 2020.

Mohammed Al-Husseini (Member, IEEE) received the Ph.D. degree in electrical and computer engineering from the American University of Beirut (AUB), Beirut, Lebanon, in 2012.

In 2013, he was a Visiting Researcher with The University of New Mexico, Albuquerque, NM, USA. He is currently a Senior Researcher and the Research Program Director with the Beirut Research and Innovation Center, Beirut, and a Lecturer with AUB. He has over 100 publications in international refereed journals and conference proceedings. His current research focus is on material characterization and the use of machine learning for the detection of underground targets. His research interests include cognitive radio, antenna design, and RF circuits.

Dr. Al-Husseini was a recipient of the Kamal Shair Ph.D. Fellowship at AUB.